The biodistribution of polystyrene nanoparticles administered intravenously in the chicken embryo

Wang, M.; Chen, S.; Cheng, S.; Nederstigt, T.A.P.; Poelmann, R.E.; DeRuiter, M.C.; ... ; Richardson, M.K.

Environment International 188 (2024) 108723

Contents lists available at ScienceDirect

Environment International

journal homepage: www.elsevier.com/locate/envint

Full length article

The biodistribution of polystyrene nanoparticles administered intravenously in the chicken embryo

Meiru Wang [a], Shuhao Chen [a], Shixiong Cheng [a], Tom A.P. Nederstigt [b], Robert E. Poelmann [a], Marco C. DeRuiter [c], Gerda E.M. Lamers [a], Joost J. Willemse [a], Chiara Mascitelli [a], Martina G. Vijver [b], Michael K. Richardson [a,*]

[a] Institute of Biology, Leiden University, Sylvius Laboratory, Sylviusweg 72, 2333 BE Leiden, The Netherlands
[b] Centrum voor Milieuwetenschappen Leiden (CML), Van Steenis Building, Einsteinweg 2, 2333 CC Leiden, The Netherlands
[c] Department of Anatomy and Embryology, Leiden University Medical Center, LUMC Onderzoeksgebouw, Einthovenweg 20, 2333 ZC Leiden, The Netherlands

ARTICLE INFO

Handling Editor: Marti Nadal

Keywords:
Nanoplastics
Trainable weka segmentation
Pharmacokinetics
Heart
Nanomedicine

ABSTRACT

Nanoplastics can cause severe malformations in chicken embryos. To improve our understanding of the toxicity of nanoplastics to embryos, we have studied their biodistribution in living chicken embryos. We injected the embryos in the vitelline vein at stages 18–19. We injected polystyrene nanoparticles (PS-NPs) tagged with europium- or fluorescence. Their biodistribution was tracked using inductively-coupled plasma mass spectrometry on tissue lysates, paraffin histology, and vibratome sections analysed by machine learning algorithms. PS-NPs were found at high levels in the heart, liver and kidneys. Furthermore, PS-NPs crossed the endocardium of the heart at sites of epithelial-mesenchymal transformation; they also crossed the liver endothelium. Finally, we detected PS-NPs in the allantoic fluid, consistent with their being excreted by the kidneys. Our study shows the power of the chicken embryo model for analysing the biodistribution of nanoplastics in embryos. Such experiments are difficult or impossible in mammalian embryos. These findings are a major advance in our understanding of the biodistribution and tissue-specific accumulation of PS-NPs in developing animals.

1. Introduction

Plastics exposed to the elements become brittle over time, and shed small particles from their surface (Weinstein et al., 2016). This surface-shedding is called delamination, and is accelerated by exposure to sunlight, warm temperatures, mechanical forces (soil movements, sea waves, etc.) and by salt water (Weinstein et al., 2016; Yee et al., 2021; Primpke et al., 2020). From these and other sources, small plastic particles can potentially enter the body through contaminated food and drink, the inhalation of airborne plastic particles, and possibly through the skin (Yee et al., 2021). Furthermore, small plastic particles are found in some types of intravenous infusion products used in medicine, providing a potential for the particles to enter bloodstream (Zhu et al., 2023; Li et al., 2023).

Small plastic particles include microplastics (MPs) whose particle size is $\leq$ 5 mm (Akdogan and Guven, 2019); and nanoplastics (NPs), whose particle size is either $\leq$ 100 nm (Ferreira et al., 2019) or $\leq$ 1 μm (Gaylarde et al., 2021; Abdolahpur Monikh et al., 2022) depending on the author. In this study, we consider 1 μm plastic particles and smaller to be nanoplastics. Nanoplastics are toxic in some animal models, including the adult mouse (Tang et al., 2023) and the embryonic chicken (Nie et al., 2021; Wang et al., 2023). In the adult mouse, polystyrene nanoplastics (PS-NPs) cause damage to the kidneys (Tang et al., 2023). In the chicken embryo, the outcomes of PS-NP exposure include malformations of the central nervous system, heart and other organs (Nie et al., 2021; Wang et al., 2023). The mechanism of PS-NP toxicity to the chicken embryo may be that they adhere selectively to neural crest cells, primitive streak, and other cell populations undergoing epithelial-mesenchymal transition (Wang et al., 2023) and then injuring those cells, possibly after the PS-NPs are taken up by endocytosis and initiate damage by inducing the production of reactive oxygen species (Zhu et al., 2023).

In order to gain a more complete understanding of the toxicity of nanoplastics to embryos, we need detailed information about their biodistribution (distribution in the living organism). This information will also be informative in the context of plans to use nanoplastics (and

* Corresponding author.
E-mail address: m.k.richardson@biology.leidenuniv.nl (M.K. Richardson).

https://doi.org/10.1016/j.envint.2024.108723
Received 7 February 2024; Received in revised form 8 April 2024; Accepted 6 May 2024
Available online 9 May 2024

other nanomaterials) as drug-delivery vehicles in the field of nanomedicine (De Jong et al., 2008; Waheed et al., 2022; Bakry et al., 2007; Chen and Feng, 2022; Rasmussen et al., 2022; Kopeček and Yang, 2020; Fernández et al., 2022; Boehnke et al., 2022) (Chai et al., 2020; Johrden et al., 2013; Kaur et al., 2010; Jia et al., 2023). One of the main administrative routes for nanomedicines is intravenous injection (Fattal and Tsapis, 2014). To date, PS-NPs have not been licensed for use in human patients.

In humans, small plastic particles have been found in tissues such as the placenta (Ragusa et al., 2021), breast milk (Ragusa et al., 2022), blood (Leslie et al., 2022), vitreous humor (Zhong et al., 2024), heart (Yang et al., 2023) and lungs (Amato-Lourenço et al., 2021). The biodistribution of PS-NPs has also been studied experimentally in adult fish (Habumugisha et al., 2023) or fish larvae (Brun et al., 2019; Hu et al., 2021), and in each case, a high concentration was found in the intestine after PS-NPs were added to the swimming water. In experimental studies on rodents, the biodistribution of nanoplastics has been studied by tagging PS-NPs with a radiolabel (Delaney et al., 2023; Keinänen et al., 2021) or fluorescent tag (Nikolic et al., 2022; Liu et al., 2023). Although several studies employed the intravenous injection route in adult rodents, those studies did not look at the biodistribution of MPs or NPs (Wang et al., 2023; Sun et al., 2022; Wei et al., 2022).

In this study, we have performed intravenous injections of PS-NPs in the chicken embryo. We used injections because it is not known whether nanoplastics cross epithelial barriers in the this model. We chose the chicken embryo itself because it is a standard model organism for studies of toxicity (Stark et al., 2019), organogenesis (Zhang et al., 2009; Ross and Smith, 1910) and developmental biology (Hamburger and Hamilton, 1951; Rashidi and Sottile, 2009). This is because of its ease of access to experimental manipulation. In this study we are using the chicken embryo to study the biodistribution of PS-NPs in a developmental system; we are not using it to make statements about the distribution of nanoplastics in adult humans. Nonetheless it is worth noting that the chicken shares a relatively high degree of genetic similarity with humans. For instance, about 60 % of chicken protein-coding genes having at least one human orthologue (Hillier et al., 2004). Duman et al. showed that the chicken embryo model can be used to mimic human tissues and can be considered as a platform for the study of teratogens (agents that cause malformations) (Duman et al., 2019). What is more, it is possible in the chicken embryo to acquire *in vivo* observations at different timepoints post-exposure (Wang et al., 2023; Wachholz et al., 2021; Butler et al., 2022). By contrast, such experiments are almost impossible in mammals for two reasons: (i) the embryo is inside the mother's uterus, surrounded by extraembryonic membranes, and therefore almost impossible to access (ii) the embryo may not be accessible to nanoplastics injected into the mother's bloodstream because they would have to cross the placental barrier.

In this study, we have made the first comprehensive, quantitative and qualitative investigation into the biodistribution of tagged PS-NPs using analysis of tissue lysates, paraffin- and vibratome histological sections. We used the chicken embryo because it is a warm-blooded vertebrate with a circulatory system that is easily accessible for intravenous injections of PS-NPs (Butler et al., 2022). Furthermore, much smaller volumes of the tagged nanoplastics are injected in the chicken embryo compared, for example, with the adult mouse (in this study, 2.5 μL of PS-NP suspension was used per chicken embryo, while 100 μL of microplastics or nanoplastics was used per adult mice (Delaney et al., 2023; Wang et al., 2023). It is important to minimise the quantities of nanoplastics used in experiments for two reasons. First, the tagged nanoplastics we used here are very expensive. Second, nanoplastics are known toxins and pollutants. We chose polystyrene nanoplastics because polystyrene is one of the most abundant waste plastics in the environment (Mendoza et al., 2020), and because PS-NPs and other microparticles have been studied as potential drug delivery agents in nanomedicine (Boehnke et al., 2022). In this study, we have injected plastic nanoparticles intravenously into the chicken embryo. This is the first time this approach has been used to study the biodistribution of plastic nanoparticles to multiple organs of the embryo. Our study provides insights into the biodistribution of nanoplastics in embryos after they enter the embryonic bloodstream.

2. Materials and methods

2.1. Preparation and synthesis of plastic nanoparticles

We used three different polystyrene nanoplastic particles (PS-NPs) in this study:

(i) **Eu-NPs:** plain (non-functionalized), 150 nm nominal diameter, 1.05 g/cm^3, 1 % solid, tagged with tris(thenoyltrifluoroacetonato)europium ($Eu(TTA)_3$), Eu 1.13 % w/w. This compound is luminescent (Binnemans et al., 2004). The particles were synthesized according to a previously described combined swelling-diffusion technique (Luo et al., 2022). For details of the synthesis, characterization and *in situ* quantification see Supplementary_File 1.

(ii) **NMF-NPs:** plain (non-functionalized), from Lab 261, Alto, U.S. cat. number FGP1000, 1.0 μm nominal diameter, 1 % solid, 1.05 g/cm^3. The particles are labelled with green florescence (Ex/Em = 460/500 nm).

(iii) **CMF-NPs:** functionalized (carboxylate-modified, Invitrogen™; cat. number F8823), 1.0 μm nominal diameter, 2 % solid, 2 mM NaN3, 1.05 g/cm^3. The particles are labelled with green florescence (Ex/Em = 505/515 nm).

Two different sizes of nanoplastics were used in this study: 150 nm and 1 μm. They therefore cover a wide size range in the nanoscale, something which is also true of nanoplastics found in the environment (Sangkham et al., 2022). We had various considerations when choosing the size of particles for our experiments. In general, smaller particles are more toxic than larger ones (Sharma et al., 2023). Furthermore, smaller particles are thought to be more easily taken up into cells than larger ones (Paul et al., 2022). Finally, the size of the particle has been shown to affect their biodistribution (in adult mice (Liang et al., 2021). In this study we chose 150 nm nanoplastics as our smaller size. However, 150 nm fluorescent nanoplastics are difficult to resolve with optical microscopy. We therefore used 1 μm NMF-NPs and CMF-NPs for our visualization experiments here. The plain and the functionalised particle were used because they are also relevant to PS-NPs environmental exposure in real life. For instance, many environmental factors including solar ultraviolet radiation and mechanical abrasion can cause carboxylation (Gewert et al., 2015; Meides et al., 2021).

We characterized all three types of NP using methods described previously (Wang et al., 2023). In brief, the size-distribution and zeta potentials of the nanoparticles suspended in Ringer's solution (pH 7, 2.5 g/L, cat. number 1.15525, Merck Millipore, Germany), were determined using multi-angle dynamic light scattering (MADLS, Malvern Panalytical Ltd., Malvern, UK). Their shape in Milli-Q® water was determined by drying the suspended particles onto 200 mesh pioloform-coated copper grids (Agar Scientific, UK) then imaging with a JEOL 1400 + transmission electron microscope (JEOL Ltd., Japan).

2.2. Intravenous injection of nanoplastics in the chicken embryo

The workflow for our experiments is summarized in Graphical abstract. We used the protocol we described previously (Wang et al., 2023). In brief, fertilised chicken eggs (*Gallus gallus*) of the White Leghorn strain were purchased from a commercial supplier (Drost Loosdrecht B.V., The Netherlands). They were incubated for 3.5 d at 38.3 °C on stationary shelves in a humidified, forced-draft incubator (Binder, Germany). Under aseptic conditions, the eggs were windowed and staged according to Hamburger and Hamilton (Hamburger and

Hamilton, 1951).

All three types of nanoparticles were suspended in Ringer's solution to yield the final concentration of 5 mg/mL (Eu-NPs), 1 mg/mL (NMF-NPs), and 2 mg/mL (CMF-NPs), respectively. We injected the same volume (2.5 μL) for all three types of nanoplastics in order to standardize the procedure as much as possible. However, we did use different concentrations of the three nanoplastic particles. The reason why we chose a higher concentration (5 mg/mL) for the Eu-NPs is because we want to detect the Eu-NPs at a relatively late developmental stage (stage 35). Such old embryos present a problem because their dramatic increase of biomass and volume of the organs will dilute the concentration of nanoplastics compared to the younger embryos.

For NMF-NPs, by contrast, we examined the injected chicken embryos at much earlier stages with lower concentrations (1 mg/mL). We used a concentration of CMF-NPs twice as high as that of NMF-NPs, because we observed fewer NMF-NPs in the tissue by paraffin sectioning in our NMF-NPs studies (Fig. 3). But we observed sufficient fluorescence signals from NMF-NPs in vibratome sections (Fig. 4). One explanation is that the paraffin sections (7 μm) are much thinner than the vibratome sections (100 μm). However, paraffin sections provide better resolution of cellular structure, compared to vibratome sections. Therefore, we decided to increase the CMF-NPs concentration (2 mg/mL) to better visualize the pattern of CMF-NPs distribution in heart paraffin section.

The nanoparticle suspensions were sonicated for 10 min in a Bransonic 12 ultrasonic cleaning bath (Branson Instruments Co., Connecticut, USA). Stage 18 or 19 embryos were injected in the vitelline vein with 2.5 μL of one of these diluted suspensions (or with Ringer's solution only as a control). We chose stage 18 or 19 to perform injections because it has been shown previously that these are optimal stages in terms of practicality and embryo survival (Hogers et al., 1995). At earlier stages, the veins are so small that it becomes extremely difficult to make the injections without damaging the embryo. At later stages the veins become inaccessible because they are overgrown by the extra-embryonic membranes. In any case, the difference between stages 18 and 19 is barely perceptible (Hamburger and Hamilton, 1951).

Each injection had a duration of c. 2.5 min. We used glass needles (Harvard Apparatus, cat. GC100F-10) pulled with a Flaming/Brown type micropipette puller (Sutter Instruments Model P-87). The needles were mounted on a Leitz-Wetzlar micromanipulator. The pressure of the injections was generated with a Picospritzer III (Parker Hannifin Corp.) with the pulse duration set at 15–25 ms. The egg was then sealed with Scotch® prescription label tape 800 (clear) and returned to the incubator.

2.3. Quantification of Eu-NPs in whole organs of the chicken embryo

2.3.1. Sampling of allantoic fluid

The Eu-NP injected eggs and controls were re-opened at 5.5 days post injection (dpi). Then, allantoic fluid from the embryos was extracted using a 1 mL Luer syringe (cat. number 2105074, BD Plastipak™, the Netherlands) with a 21G needle (0.8 × 40 mm, BD Microlance™ 3 needles, Switzerland) *in ovo*. A fresh syringe and needle were used for each embryo. A total volume of 200 μL of allantoic fluid was transferred from each embryo into separate 15 mL falcon tubes (cat. number 525–1085, VWR™).

2.3.2. Heparin-PBS flushed embryos

Some of the embryos injected with Eu-NPs (and their Ringer's-only controls) were first flushed with a heparin solution, to remove blood from the tissues, before they were fixed. The heparin solution (heparin sodium salt, cat. number A3004,0001, AppliChem Panreac) 100 IU/mL in phosphate-buffered saline (PBS), was pre-warmed to 38 °C. Intact embryos were placed into a Petri dish containing the warm heparin solution. Blood was then flushed from the tissues by injecting the embryo with warm heparin solution in the heart, using a 1 mL Luer syringe fitted with a 30G needle. Tissues from these flushed embryos were otherwise dissected out and processed exactly as described for the non-flushed tissues (above and below).

2.3.3. Dissection of tissues from the chicken embryo

Treated and control embryos were harvested at 5.5 dpi and fixed in 4 % buffered depolymerised paraformaldehyde (pFA) overnight at 4 °C. They were then rinsed in refresh cold PBS on a rotator (RS-TR05, Phoenix Instrument, Germany) for 2 d at 4 °C. Then, embryos were moved into a clean plastic Petri dish, and dissected using Dumont watchmaker's forceps (cat. number 11251–30) and student Vannas Spring Scissors (cat. number 91500–09) both from Fine Science Tools, Switzerland. The tissues dissected were: heart, liver, kidney, intestine, brain, eye and lung. After the dissection, each sample was transferred individually with a microspoon, 6 mm bowl width, with as little adherent PBS as possible, to a clean, pre-weighed, 15 mL Falcon tube. The wet weight of the individual tissues was then measured using an analytical balance (cat. number PRACTUM124-1 s Sartorius GmbH, Germany).

2.3.4. Dry weight determination and tissue digestion

The tissue samples (or a 200 μL aliquot of allantoic fluid) were dried at 68 °C and their dry weight determined using an analytical balance. Subsequently, the samples were digested in an 8:1 mixture of HNO_3: H_2SO_4 (v/v) at 70 °C for 24 h.

2.3.5. Eu-NPs measurement and data analysis

Tissue and allantoic fluid samples of flushed and non-flushed embryos (5.5 dpi) were quantified by proxy from ^{153}Eu concentrations measured using inductively coupled plasma mass spectrometry (ICP-MS, PerkinElmer NexION 300D, PerkinElmer, Waltham, Massachusetts, United States). Factorial anovas (R, v. 4.3.1., R Core Team 2021, package: *stats*, function: *aov*) followed by pairwise comparisons of estimated marginal means (package: *emmeans*, function: *emmeans*) were used to determine: i) differences between signals obtained from samples derived from exposed- and non-exposed embryos; ii) differences in Eu-NP concentrations between organs derived from flushed- and non-flushed embryos; iii) differences in Eu-NP concentrations between different organs. Tissue concentrations were considered quantifiable when signals from samples derived from exposed embryos showed a statistically significant ($P < 0.05$) increase relative to those of samples derived from non-exposed individuals. ^{153}Eu concentrations were converted to Eu-NP concentrations based on analytically determined mass percentages of Eu incorporated into the polymer matrix of the particles. Tissue concentrations were corrected for mean background signals (i.e. signals from samples derived from Ringer's control embryos) which were obtained from equivalent numbers of replicates ($n = 6$) for each tissue. All models were assessed for relevant assumptions, p-values derived from post-hoc analyses were corrected for false-discovery rates and analyses were performed using R version 4.3.1.

2.4. Real-time video recording in ovo

2.4.1. Imaging of chicken embryos injected with Eu-NPs

The recordings were made under 365 nm UV excitation from an external fluorescence light source, excitation EL6000 (Supplementary_Fig. 1). The excitation filter (cat. 365WB50, Omega Optical, LLC, Brattleboro, USA) was fixed inside a 50 mL Falcon tube from which the bottom had been cut off. The light source was shone into the opposite end to the filter in the 50 mL Falcon tube. The recordings were made with the same Nikon stereo microscope and Dino-Eye eyepiece camera described in the previous section. For recordings made during the Eu-NPs injection, see (Supplementary_Video 1, Supplementary_Video 2).

2.4.2. Imaging of chicken embryos injected with NMF-NPs and CMF-NPs

We have described the protocol in a previous study (Wang et al.,

2023). Briefly, video recordings were performed under light emitted by a fluorescence excitation light (model SFA, Nightsea, Hatfield, PA) with a Nightsea SFA yellow barrier filter in front of a Nikon SMZ1500 stereo microscope fitted with a Dino-Eye eyepiece camera (Dino-Lite Europe, Almere). Videos of NMF-NPs injections were recorded at 24 hpi (Supplementary_Video 3) and 48 hpi (Supplementary_Video 4). For the CMF-NPs injections, videos were recorded at 0 hpi (Supplementary_Video 5) and 24 hpi (Supplementary_Video 6).

2.5. Paraffin histology

2.5.1. Paraffin embedding

Embryos were dehydrated, embedded in paraffin and sectioned according to standard protocols and as previously described by us (Wang et al., 2023). Briefly, stage 25 (1.5 dpi) or 28 (2.5 dpi) embryos were fixed in 4 % pFA for 24 h at 4 °C. They were then washed 3 × with cold PBS and dehydrated in 70 % ethanol overnight. Subsequently, the embryos were dehydrated through a graded ethanol series (80 %, 90 %, 100 %), 1 h each. Embryos were cleared with NeoClear® (Merck, Darmstadt), 3 × 1 h, and embedded in paraffin (Paraclean histology wax, KP Klinipath/VWR International, Amsterdam) at 60 °C (1 × overnight, then 1 × 1 h). Sections were cut at 7 μm and mounted on glass microscope slides. For the dewaxing of the sections we slightly modified the standard protocol (Gamble et al., 2008). Slides were immersed in NeoClear® for 30 min × 3 at 60 °C in the incubator. They were then rehydrated through a descending series of ethanols: 100 % 3 x, then 1 × each of 90 %, 80 % and 70 % ethanol.

2.5.2. Haematoxylin, eosin and Alcian blue staining

Slides were washed in PBS and stained with haematoxylin and eosin according to Gamble (Gamble et al., 2008). Sections of the embryo were additionally stained with Alcian blue (1 % aqueous). After staining, slides were rinsed in demi-water for 10 min, and a cover slip applied with 99.5 % glycerol as the mounting medium. The edges of the coverslip were sealed with nail polish. The sections were imaged using a Zeiss Axio Imager.M2 microscope.

2.5.3. DAPI and WGA staining

Paraffin sections were deparaffinised and rehydrated as described above. They were then transferred to PBS. In order to reduce the autofluorescence of the tissue, the TrueVIEW autofluorescence quenching kit (Vector Laboratories, Inc., USA, cat. SP-8400–15) was used according to the manufacturer's instructions. In brief, 150 μL of a mix containing equal volumes of reagents A, B and C were added to the one slide for 5 min. After rinsing in PBS, the slides were stained with 4′,6-diamidino-2-phenylindole (DAPI: Invitrogen, USA, cat. 23672 W) diluted with PBS to a final concentration of 5 μg/mL for 10 min. The slides were then rinsed again in PBS for 10 min, and stained with fluorescently-labelled wheat germ agglutinin (WGA: Biotium, Inc; CA, cat. CF®594 WGA) diluted with PBS to yield final concentration 5 μg/mL. Finally, the slides were washed in PBS for 10 min, and mounted with VECTASHIELD Vibrance® antifade mounting medium from the autofluorescence quenching kit. The stained sections were imaged using a Nikon AX confocal microscope.

2.6. Vibratome sections

Embryos processed for vibratome sections were stored in 0.5 % pFA (4 % pFA diluted with PBS) overnight. They were submerged in a mixture of 30 % bovine serum albumin, 20 % sucrose and 1 % gelatine (cat. number 48722, Merck Millipore, Germany) in PBS as previously described (Wang et al., 2023). The NMF-NP-injected embryos were then placed in 3 mL of fresh mixture in plastic embedding moulds and 1200 μL of formaldehyde solution (37 %–41 %) was added as a hardener. The moulds were stored at 4 °C for 5 d. The CMF-NP-injected embryos were handled slightly differently in that they were then placed in 3 mL of fresh mixture in plastic embedding moulds and 240 μL of 10 % glutaraldehyde added as a hardener. The moulds were stored at 4 °C overnight. In both cases, the tissue blocks were taken out of the moulds then trimmed and sectioned at 100 μm in Milli-Q® water and stained with 5 μg/mL DAPI. Finally, the sections were mounted on glass microscope slides with 99.5 % glycerol and examined with a Nikon AX confocal microscope.

2.7. Trainable weka segmentation

The Fiji-ImageJ plugin: *trainable weka segmentation* was used to analyse confocal images of the vibratome sections. The steps were as follows: (i) first, the ND2.* image file from the confocal microscope was imported to Fiji and summed with z-project. Selection tools were then used to select the area of interest in the z-projection; (ii) the following algorithms were selected for the classifier: *Gaussian blur*, *Sobel filter*, *Hessian*, *difference of Gaussians*, and *membrane projections*. The samples were manually classified into **class one** (particles) or **class two** (background/tissue only); (iii) the classifier was trained with the selected samples until all the particles on the images were recognized by the classifier; then the classifier was saved and a probability map generated; (iv) the threshold of the probability map was set (95–100 %) and a mask of the probability map made from 95 %; (v) the image calculator was used to extract PS-NPs from the image stack; (vi) the integrated density of the fluorescence was measured by applying the *measure* function to the image extracted in step v; (vii) the area of the selected region was measured. For more details on this workflow see Supplementary_File 2.

2.8. Scanning electron microscopy

Chicken embryos were harvested into PBS then the hearts were flushed with heparin solution (heparin sodium salt, cat. number A3004,0001, AppliChem Panreac) 100 IU/mL in PBS, pre-warmed to 38 °C, to remove blood cells from the cardiac lumen. The hearts were then perfused-fixed with 1.5 % glutaraldehyde in 0.1 M sodium cacodylate buffer (pH = 7.4) at room temperature. The hearts were stored in the fixative for 2 h then at 4 °C for 22 h. The hearts were then dissected open using iridectomy scissors to expose the luminal aspects of the outflow tract cushions. They were dehydrated in a graded ethanol series and critical-point dried over CO_2 in a Bal-Tec critical point drier 030 (Bal-Tec, Switzerland). The specimens were then mounted on aluminium stubs using carbon tape and silver glue, and sputter-coated with palladium and platinum using a Q 150 T S Plus Sputter Coater (Quorum, United Kingdom). The specimens were imaged using a Jeol JSM-7600F field emission scanning electron microscope.

3. Results

3.1. Characterization of three types of nanoplastics

All three types of plastic nanoparticles were spherical under TEM. The size distribution of the particles in Ringer's solution is shown in Fig. 1. The average size of Eu-NPs, and NMF-NPs, CMF-NPs was 171.53 ± 1.21, 1145.67 ± 112.66, and 1215 ± 112.66 nm, respectively (Fig. 1). The zeta- (ζ-) potentials were −23.98 ± 1.42, −11.41 ± 2.20, and −42.09 ± 1.97 mv, respectively.

3.2. Eu-NPs selectively accumulate in liver, kidneys and heart tissue

Eu-NP values were determined in different tissues at 5.5 dpi (Supplementary_Table 1). For Eu-NP-injected, non-flushed embryos, Eu-NPs concentrations were significantly elevated from controls in most tissues except the intestine (Fig. 2a). This was also true in the heparin-flushed embryos for kidneys, heart, liver, brain, and eye tissues; however, the Eu-NPs concentrations did not significantly differ from controls for the intestine and lung tissues (Fig. 2b). Interestingly, Eu-NP levels were particularly high in liver, kidney and heart tissues in both non-flushed

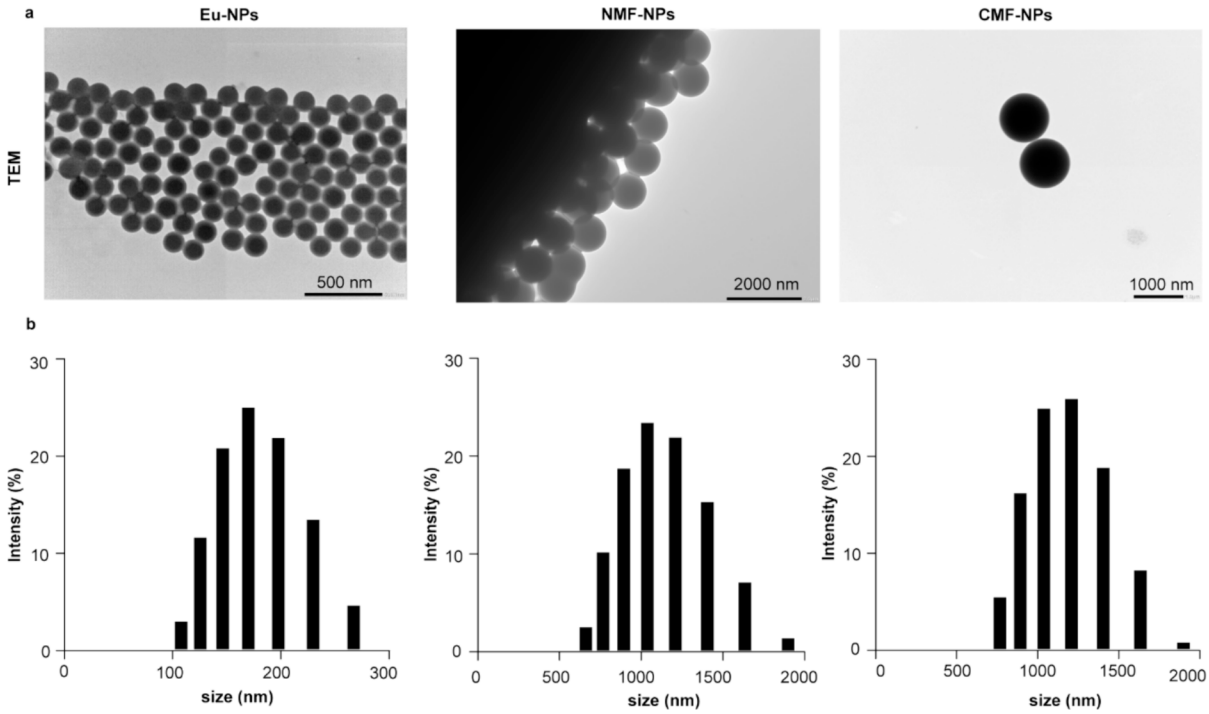

Fig. 1. Physical characterization of the three types of plastics nanoparticles used in this study. **a**, transmission electron micrographs (left to right) of Eu-NPs (150 nm), CMF-NPs (1000 nm) and NMF-NPs (1000 nm) in Milli-Q® water. The particles are seen to be spherical. **b**, size distribution of the same three types of NP in Ringer's solution measured by multi angle dynamic light scattering (MADLS). The average actual diameter of Eu-NPs, NMF-NPs, and CMF-NPs in Ringer's solution is 171.53 ± 1.21, 1145.67 ± 112.66, and 1215 ± 112.66 nm, respectively.

and flushed embryos (Fig. 2a, b).

We corrected for background signals by analysing tissue from Ringer's-only (control) injections. We found, in both non-flushed and flushed embryos, the levels of Eu-NS, corrected for background, are significantly higher in the kidneys, heart, and liver than in the other tissues analysed (Fig. 2d and e). In addition, in the heparin-flushed and background-corrected samples, the Eu-NP levels in brain tissue was statistically significantly higher than in the intestine and lung tissues (Fig. 2e). In all cases of Eu-NP injections corrected for background, the liver tissue showed the highest concentration of all seven tissues types, in the both non-flushed ($1.4e^{11} \pm 2.6e^{10}$ particles g^{-1} dw) and flushed ($1.1e^{11} \pm 4.6e^{10}$ particles g^{-1} dw) embryos (dw = dry weight).

3.3. *Eu-NPs are found in allantoic fluid*

The allantois receives the fluid secretion of the developing kidneys (in our specimens, the mesonephroi) and so, allantoic fluid is effectively urine produced by the embryo (Wenz et al., 1992) and refs. therein). We quantified Eu-NP levels in the allantoic fluid and found a strong Eu-NP signal in Eu-NP-injected embryos (equivalent to $1.0e^{9} \pm 2.6e^{8}$ particles mL^{-1}) compared to Ringer's only controls (value; $P = 8.8e^{-5}$ particles mL^{-1}; see Fig. 2c).

3.4. *Spatial biodistribution of fluorescent NPs in tissue sections is consistent with the biodistribution of Eu-NPs*

Paraffin sections of embryos injected with fluorescent NMF-NPs, and fixed at stage 25 (Fig. 3), show fluorescent particles distributed in all tissues examined. For most tissues, it was not possible to determine whether the NPs were inside capillaries in the mesenchymal tissues, or had actually undergone extravasation and passed into the extracellular space. To quantify the tissue distribution we used confocal microscopy and Trainable Weka Segmentation on vibratome sections (of embryos fixed at stage 28). NMF-NPs were detected in all seven organs studied with EU-NPs (Fig. 4).

3.4.1. *Stage 25 embryos*

NPs are seen in the neural tube (Fig. 3) and in the vasculature of the developing kidney mesonephros (Fig. 3). In the liver, and in the trabeculated region of the cardiac ventricle, PS-NPs are seen on the surface, and apparently in the cytoplasm, of endothelial cells (Fig. 3). In the eye, no NPs were observed (in the sections examined; see Fig. 3). In the lungs, NPs were seen in the mesenchyme surrounding the developing bronchi (Fig. 3); they were also seen in the gut mesenchyme (Fig. 3).

3.4.2. *Stage 28 embryos*

NPs are seen in the neural tube and the surrounding mesenchyme at this stage (Supplementary_Fig. 2). Many NPs are seen in the cardiac cushion tissue and the ventricular trabeculae (Supplementary_Fig. 2), specifically on or in endocardial cells covering the trabeculae, and at the interface between the cardiomyocytes and endocardial cells (Supplementary_Fig. 2). In the mesonephros, NPs appeared to be preferentially located in the blood vessels (Supplementary_Fig. 2) including the glomerulus. In the liver, NPs were seen on the apical surface of the endothelium, and in the space of Disse between the endothelium and the underlying hepatocytes in the liver plates (hepatic laminae or liver cords;). In the lung, the picture is similar to stage 25 (see above), with NPs in the mesenchyme surrounding the bronchial tree, but not in the epithelium of the bronchi (Supplementary_Fig. 2). In the eye, NPs were scarce, except in the neural crest-derived mesenchyme surrounding the optic cup (Supplementary_Fig. 2). As at stage 25, the stage 28 embryo shows NPs in the gut mesenchyme but not the gut epithelium (Supplementary_Fig. 2). Quantification of NP fluorescent intensity was performed at this stage (Supplementary_Fig. 2); it showed significantly higher fluorescent intensity in kidneys, heart, and liver than in the other tissues. The rank intensity was kidneys > [heart = liver].

3.5. *CMF-NPs can cross the endocardial layer of the embryonic heart*

CMF-NP-injected embryos were fixed and sectioned (vibratome and paraffin sections) at stages 25 and 28 (Fig. 5). We found CMF-NPs in the

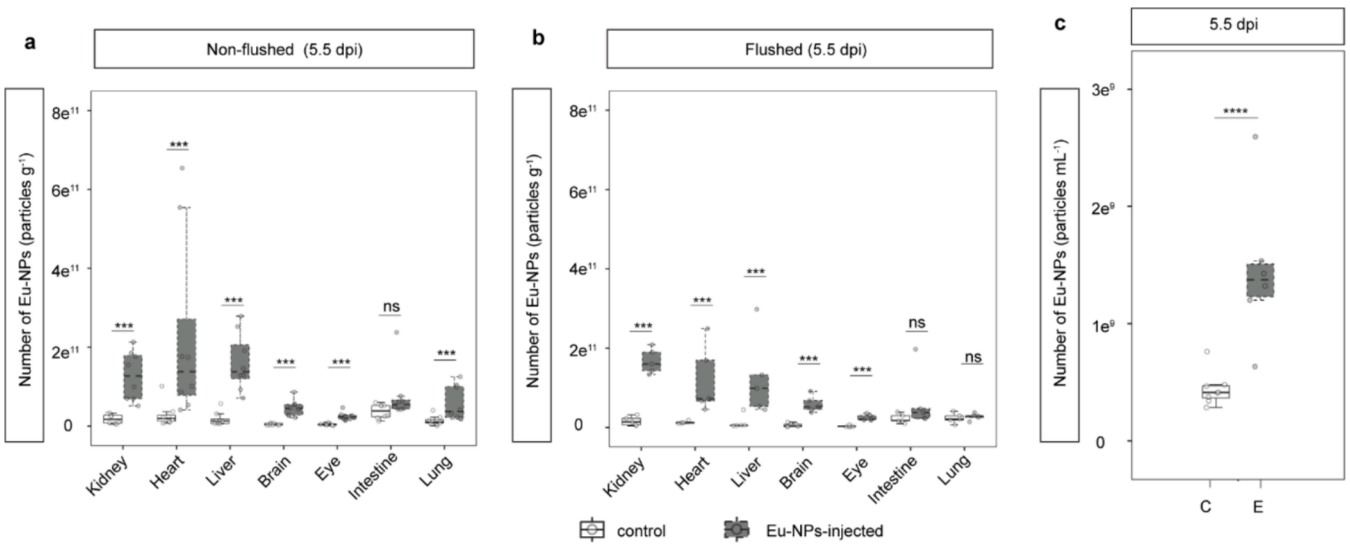

d

Non-flushed (5.5 dpi)

p	Heart	Liver	Brain	Eye	Intestine	Lung
Kidney	0.92	0.73	0.16	0.01	0.01	0.03
Heart		0.77	0.13	0.01	0.01	0.02
Liver			0.05	$7.4e^{-3}$	$7.4e^{-3}$	0.01
Brain				0.33	0.30	0.53
Eye					0.92	0.80
Intestine						0.77

e

Flushed (5.5 dpi)

p	Heart	Liver	Brain	Eye	Intestine	Lung
Kidney	0.49	0.49	0.17	0.01	$2.0e^{-4}$	$2.0e^{-4}$
Heart		0.99	0.52	0.08	$1.0e^{-3}$	$1.0e^{-3}$
Liver			0.52	0.08	$1.0e^{-3}$	$1.0e^{-3}$
Brain				0.27	$7.0e^{-3}$	$7.0e^{-3}$
Eye					0.13	0.11
Intestine						0.89

Fig. 2. Eu-NPs biodistribution in chicken embryo and allantoic fluid. a, comparison of the concentration of Eu-NPs in seven organs in control (Ringer's only injection) and experimental (Eu-NPs-injected) chicken embryos at 5.5 d post exposure (dpi; both groups were non-flushed). $n = 6$ for both control and Eu-NPs-injected groups. **b**, concentration of Eu-NPs in seven organs in control and Eu-NPs-injected chicken embryos at 5.5 dpi (both groups were flushed). $n = 6$ for both control and Eu-NPs-injected groups. **c**, concentration of Eu-NPs in the allantoic fluid of control and Eu-NPs-injected chicken embryos at 5.5 dpi. $n = 8$ for control group and $n = 6$ for Eu-NPs-injected group. For **a**–**c**, data are mean ± s.e.m. **d** and **e**, comparison of Eu-NPs concentration between dissected organs in non-flushed and flushed groups ($n = 6$ for both groups; both concentration were background corrected), along with their statistical significance. Significance of difference between organs indicated in **a**–**c** by asterisks as follows: (****, $P < 0.0001$; ***, $P < 0.001$; **$P < 0.01$; *$P < 0.05$, ns for $P > 0.05$.). In **d** and **e**, the significance were indicated by gradient colours as follows: ■, $P < 0.0001$; ■, $P < 0.001$; ■, $P < 0.01$; ■, $P < 0.05$). Detailed statistic analysis is shown in Supplementary_File 3.

endocardial epithelium overlying the endocardial cushions in stage 25 (Fig. 5a, b; Supplementary_Video 7). Later, at stage 28, we saw CMF-NPs in the body of the endocardial cushions, among the mesenchymal cells and their matrix (cardiac jelly; Fig. 5c–h). NPs were seen in the cushions along the length of the outflow tract. Qualitatively, there is the appearance of uptake or migration of PS-NPs particularly in the parietal and medial cushions (Fig. 5c, d). Moreover, we also found CMF-NPs in the aortico-pulmonary septal complex (Fig. 5e, f) and interventricular septum (Fig. 5h).

We conducted scanning electron microscopy of normal stage 19 chicken embryo hearts, cut open to expose the interior (Fig. 5). This showed 0.75–4 μm diameter holes or fenestrae between the cells of the endocardium overlying the outflow tract cushions (Fig. 5). The fibrillar material of the cardiac jelly is visible in the floor of the fenestrae.

4. Discussion

We have studied the experimental biodistribution of europium-tagged and fluorescence-tagged polystyrene nanoparticles (PS-NPs) injected intravenously into the vitelline vein of stage 18 or 19 chicken embryos. The embryos were analysed at a range of stage post-injection to see if the biodistribution of nanoplastics was influenced by the stage of organ development. We find that nanoplastics preferentially accumulate in the kidneys, heart and liver. This finding is consistent with studies on adult mice (Delaney et al., 2023). We also make several major new findings: (i) PS-NPs can cross endothelia in the heart and liver; (ii) PS-NPs accumulate in the embryonic urine (allantoic fluid) suggesting that they might be excreted by the developing kidneys; (iii) the biodistribution pattern of 150 nm PS-NPs is similar to that of 1 μm PS-NPs; (iv) flushing the blood vessels out with buffer does not make a significant difference to the concentration of PS-NPs in tissues and organs. This suggests that the concentration of PS-NPs in the blood does not influence the concentrations recorded in the tissue samples.

This study is the first to report the biodistribution of nanoplastics in the chicken embryo injected intravenously. Such an experiment is difficult or impossible in mammalian embryos due to the placental barrier and the closed environment in which the embryo grows (enclosed in extraembryonic membranes and in the uterus). Previous studies of the biodistribution of non-plastic nanomaterials in mice used adult stages, not embryos (reviewed in (Kumar et al., 2023). Those studies found preferential accumulation in the liver, spleen and kidneys, with lower levels in the brain after intravenous administration into adult mice (Kumar et al., 2023).

Other studies focused on the biodistribution of nanoplastics and microplastics in adult mice after experimental administration by oral feeding (Liang et al., 2021) or inhalation (Delaney et al., 2023). In one such study using adult mice, nanoplastics were highly distributed in the intestine, spleen, kidney, heart and liver (Liang et al., 2021) after oral feeding. In our study, we also found high concentrations of nanoplastics in the organs of heart, liver, kidneys, but not intestine. The fact that we found relatively low levels of particles in the intestine, compared to the mouse study (Liang et al., 2021) might be because the latter study involved oral administration of the nanoparticles.

Similar considerations may explain why studies of zebrafish adults or larvae (Habumugisha et al., 2023; Brun et al., 2019; Hu et al., 2021), exposed to nanoplastics in their swimming water, showed accumulation

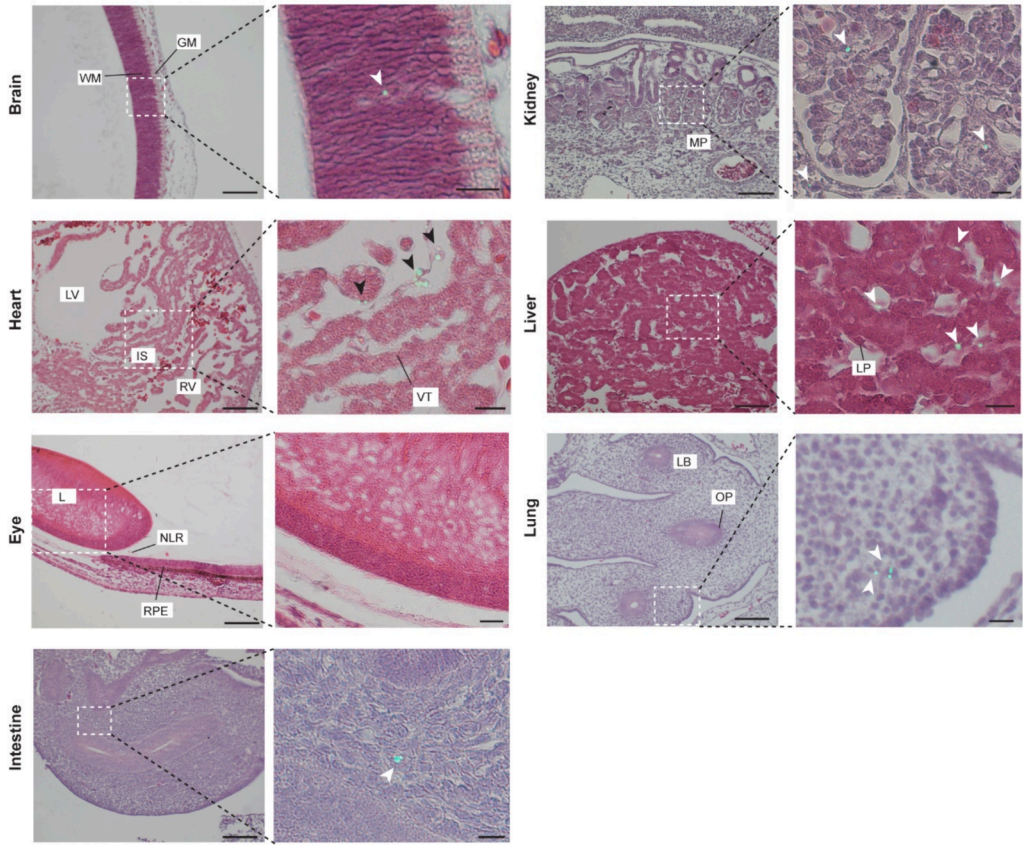

Fig. 3. Tissue distribution of NMF-NPs examined at stage 25 (1.5 dpi). The 1 μm Φ plastic nanoparticles (NMF-NPs; Ex/Em = 460/500 nm) are indicated by green fluorescence. $n = 2$ for individuals. *Key*: arrowheads, NMF-NPs; GM, grey matter; IS, interventricular septum; L, lens; LP, liver plate; LB, lung bud; LV, left ventricle; MP, mesonephros; NLR, neural layer of retina; OP, oesophagus; RPE, retinal pigment epithelium; RV, right ventricle; V, ventricle; VT, ventricular trabeculae; WM, white matter. Scale bars are 50 μm in low magnification images, and 10 μm in the enlarged views. (For interpretation of the references to colour in this figure legend, the reader is referred to the web version of this article.)

of the particles in the digestive tract. In the first of these three studies (Habumugisha et al., 2023) the relative rank biodistribution of administered nanoplastics in the zebrafish adult was intestine > liver > gill > muscle > brain. In the second study (Brun et al., 2019) PS-NPs accumulated in the intestine, exocrine pancreas, and gallbladder of exposed zebrafish larvae. In the third study, PS-NPs were mainly distributed in the liver, stomach, intestine, pancreas and gall bladder of exposed zebrafish larvae (Hu et al., 2021).

Here, we used nanoplastics with two different types of taggant: europium-based and fluorescence-based), different functionalization and different sizes (150 nm and 1 μm PS-NPs). We found that size and taggant characteristics did not influence the biodistribution in the chick embryo. This is in contrast to a study of adult mice, where the size of the nanoparticle did affect the biodistribution (Liang et al., 2021).

We also observed relatively low levels of NPs in the central nervous system (CNS, or neural tube in the embryo). One possible explanation is that NPs are excluded from the CNS by the blood–brain barrier. However, the blood–brain barrier may not be functional in the chicken at the stages we examined. Thus, one study (Wakai and Hirokawa, 1978) using horseradish peroxidase to probe the blood–brain barrier found that it was not functional until stages 39–41. Even if a blood–brain barrier has developed at the stages we studied, NPs may be able to cross it. For example, in a study of adult mice, 50 nm polystyrene NPs were found to cross the blood–brain-barrier (Shan et al., 2022). It is also important to consider that the size of plastic particles may be a critical factor in determining their ability to cross the blood–brain barrier (Kopatz et al., 2023). In any case, at the stages we examined here, the blood–brain barrier is not yet formed; the chicken embryo does not have a completely formed blood–brain barrier until very late stages (stage 41 – see Wakai and Hirokawa, 1978), which is around 15 days incubation (Hamburger and Hamilton, 1951). It has already been reported that nanoplastics can cross the blood–brain barrier (Shan et al., 2022) in adult mice. It will be very interesting to determine at what stages nanoplastics of particular sizes can pass through the blood–brain barrier in the chicken embryo.

We observed relatively few NPs in the eye of exposed chick embryos. This might be explained by the fact that the vitreous cavity of the eye contains no blood vessels (Ranchod et al., 2010). Our finding is in contrast to studies in adult humans which report finding microplastics in the vitreous humour of the eye (Zhong et al., 2024).

How do we explain the high levels of PS-NPs we observed in the kidneys, liver and heart? One possible explanation is that the PS-NPs levels reflect PS-NPs in the blood inside blood vessels (and not PS-NPs that have crossed vessel walls into the tissues). If this were the case, then highly vascular tissues, which have a large blood volume, would register high levels of NPs. To examine this hypothesis, we measured Eu-NP levels in organs harvested from embryos whose vasculature had either (i) been flushed with heparin-Ringers, to remove blood or (ii) not flushed. We found that Eu-NP levels were consistently high in liver, kidneys and heart tissues in both flushed and non-flushed embryos (Fig. 2a, b). The differences between flushed and non-flushed embryos were not significant. Together, these findings suggest that it is not simply a larger blood volume in those tissues which explains their high levels of PS-NPs. Another factor that may produce high levels of PS-NPs in tissues is the surface area of endothelium to which PS-NPs can adhere. For example, the ventricle of the heart has, in part, a spongy interior due to the presence of numerous muscular bundles (trabeculae carneae (Fatemifar et al., 2019), which start to develop in the chicken around stage 17 (Ben-Shachar et al., 1985).

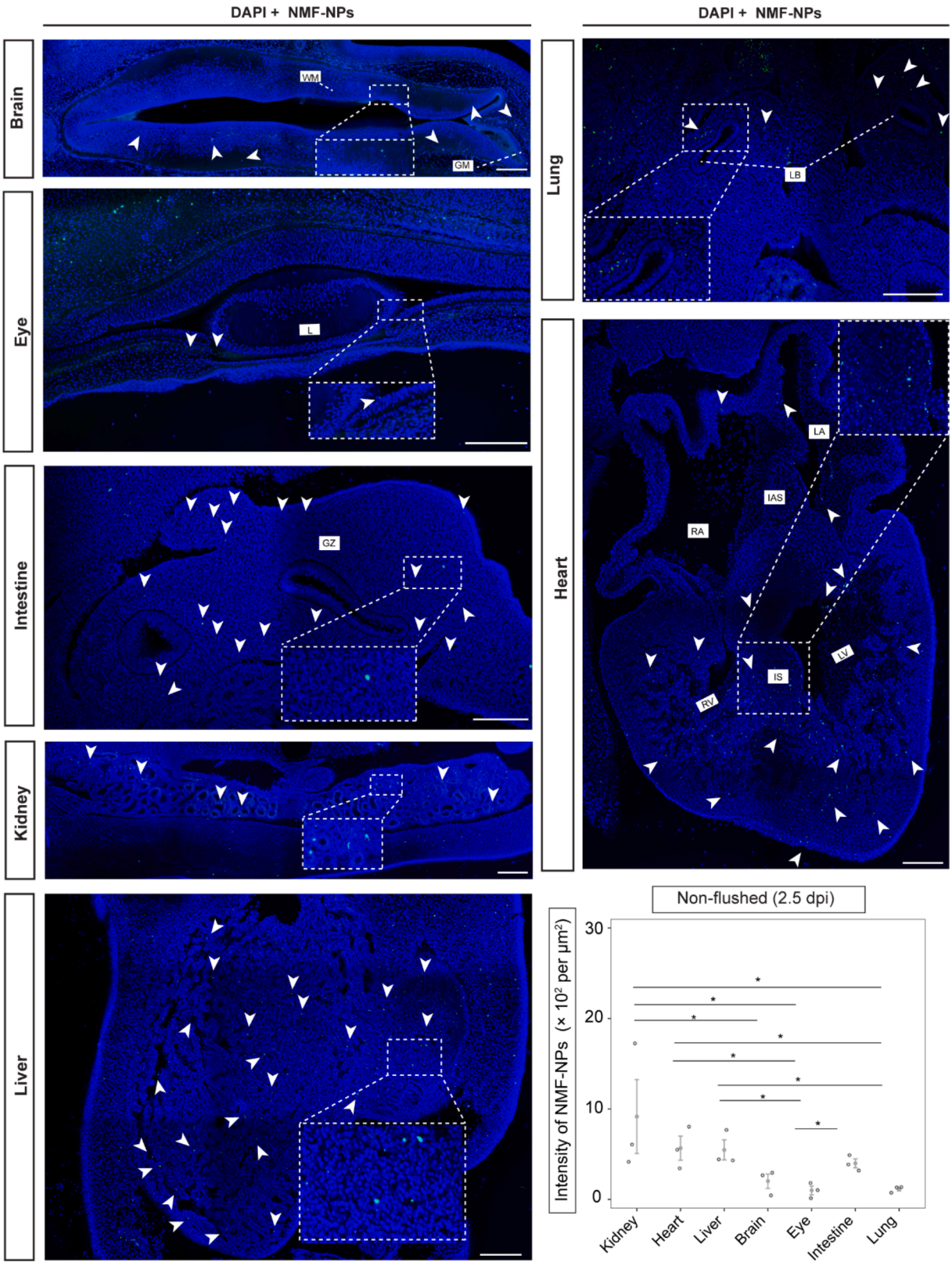

Fig. 4. Tissue distribution of NMF-NPs examined at stage 28 (2.5 dpi). Vibratome sections of seven organs. $n = 3$ for vibratome sections. The vibratome sections were stained with DAPI (blue) for cell nuclei. The 1 μm ø plastic nanoparticles (NMF-NPs; Ex/Em = 460/500 nm) are indicated by green fluorescence in vibratome sections. *Note*, white arrowheads have been selectively used to indicate examples of NMF-NPs. Graph (bottom right) indicates the fluorescence intensity of NMF-NPs that examined in the vibratome section analysed by Trainable Weka Segmentation ($n = 3$ for individuals; $n = 3$ for the slides number for each individual). Data are mean ± s.e.m. The statistical significance between organs indicated by asterisks as follows: $^*P < 0.05$. *Key*: GM: grey matter; GZ: gizzard; IAS: interatrial septum; IS: interventricular septum; L: lens; LA: left atrium; LB: lung bud; LP: liver plate; LV: left ventricle; MP: mesonephros; NLR: neural layer of retina; RA: right atrium; RV: right ventricle; V: ventricle; WM: white matter. Scale bars in vibratome sections, 200 μm. (For interpretation of the references to colour in this figure legend, the reader is referred to the web version of this article.)

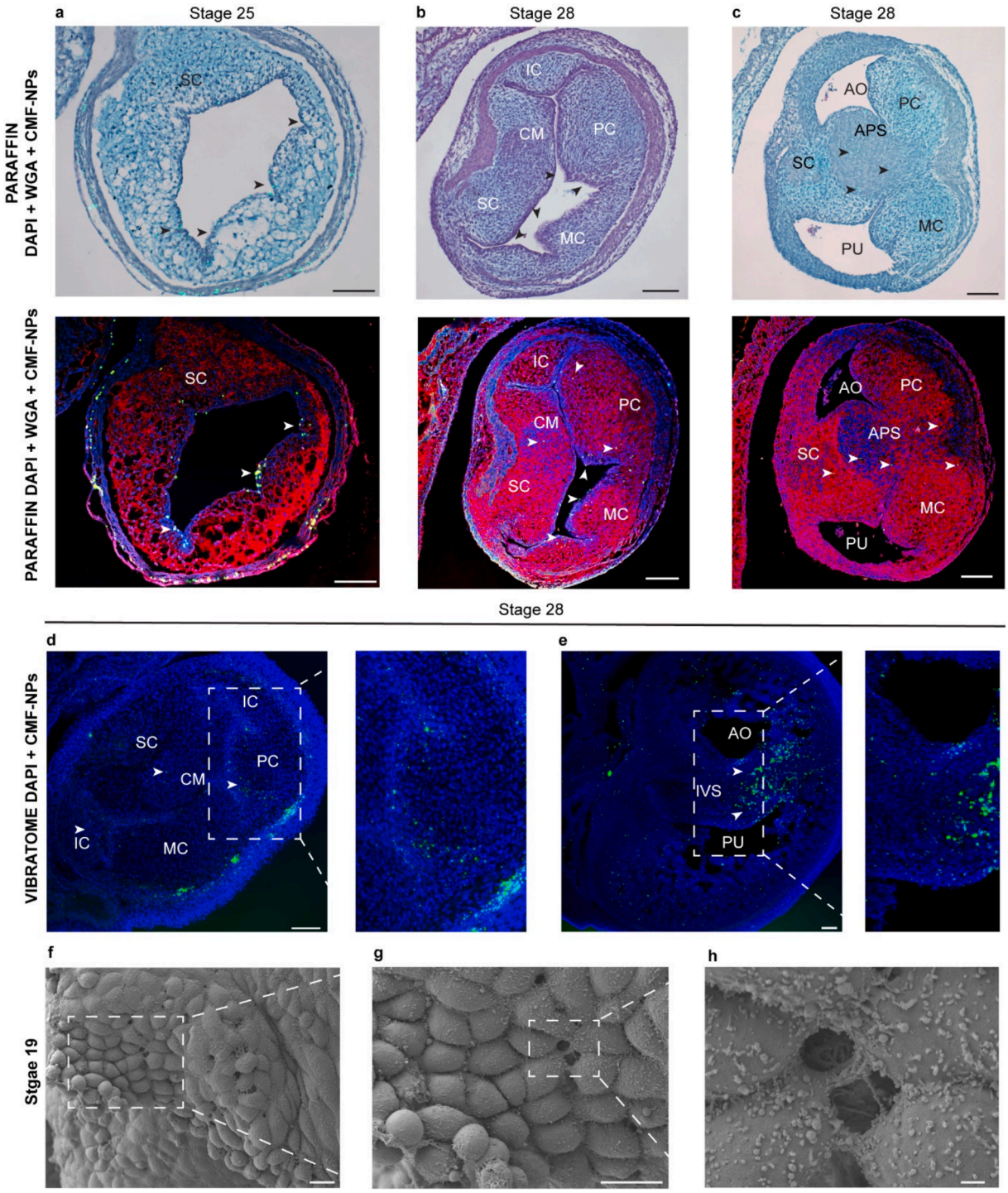

Fig. 5. Nanoplastics and the chicken heart. a–e, biodistribution of CMF–NPs in the chicken heart tract at stages 25–28 (1.5–2.5 dpi). Sections with white background are paraffin sections stained with haematoxylin and eosin ($n = 2$); sections with bright red tissue and black background are paraffin sections double–stained with DAPI and wheat germ agglutinin ($n = 2$); sections with dark blue tissue and black background are vibratome section stained with DAPI only ($n = 3$). b, c, transverse sections through the outflow tract of the same embryo. b, distal outflow tract, and c, proximal outflow tract. for both stage 25 and stage 28. d, vibratome section at stage 28. e, vibratome section of interventricular septum. The 1 μm Φ plastic nanoparticles (CMF–NPs; Ex/Em = 505/515 nm) are indicated by green fluorescence in both vibratome and paraffin section. Note, black and white arrowheads indicate the CMF-NPs. f–h, SEM imaging of outflow tract cushions (stage 19). f, lower magnification of the surface of the endocardium. g, boxed area from f, showing several fenestrae (arrowheads). h boxed area from g showing two fenestrae 2–3 μm in maximum diameter. In the floor of the fenestrae the fibrils of cardiac jelly can be seen (there is no basal lamina in the endocardial cushions). Key: AO: aorta; APS: aortopulmonary septum; CM: condensed mesenchyme cells; IC: intercalated cushion; IVS: interventricular septum; MC: medial cushion; PC: parietal cushion; PU: pulmonary; SC: septal cushion. Scale bars are 100 μm in a–e, 10 μm in f and g, and 1 μm in h. For the anatomy of the cardiac cushions, see (Qayyum et al., 2001). (For interpretation of the references to colour in this figure legend, the reader is referred to the web version of this article.)

Another explanation for the relatively high levels of PS-NPs we observed in the heart, liver and kidneys is that the endothelium is specialised in a way that favours NP adherence or extravasation. The kidneys and liver endothelia are specialised for the exchange of molecules (Wan et al., 2022; Choudhury et al., 2022). For this purpose, liver sinusoidal endothelial cells have holes or fenestrae (Wan et al., 2022; Braet and Wisse, 2012) which, we suggest, could provide sites for NP-transfer. In the kidneys, podocytes (Tian et al., 2022) in the visceral epithelium of the renal corpuscle also show fenestrae (filtration pores) (Rice et al., 2013; Grinstein et al., 2013). In addition to possessing fenestrated endothelia, the kidneys and liver also contain phagocytic cells. These are the mesangial cells of the renal corpuscle (Kessel and Kardon, 1979) and the Kupffer cells of the liver (Kessel and Kardon, 1979; Li et al., 2023). Both of these two cell types can take up NPs by phagocytosis (Chen et al., 2017). In addition to these specialised phagocytic cells, there are several types of phagocytic cell in the innate immune system that regularly cross capillary walls in all parts of the body by a process called diapedesis (Kamei and Carman, 2010). This 'trafficking' of phagocytic cells takes place even in healthy tissues and could be another possible mechanism of NP biodistribution; further work is needed to investigate this possibility.

We show here that the endocardium of the developing heart is also fenestrated in some regions overlying of the outflow tract cushions. These fenestrae were first observed by two of us (MDR and RPE) in unpublished studies; we can also see fenestrae overlying the atrioventricular cushions in Figs. 2, 5A-D and 6 of Manner and Merkel, 2007. We suggest that the fenestrae correspond to areas where epithelial-mesenchymal transformation (EMT) is taking place in the cushion endocardium (Markwald et al., 1977).

In this connection, it is particularly significant that we found multiple CMF-NPs inside the cushions. Since the cushions are avascular, we have to assume that the PS-NPs entered the cushions by crossing the endocardium. This hypothesis is supported by the timing of events: NPs are found on the apical surface of the endocardial epithelium at stage 25, and in the body of the cushion tissue at stage 28. Interestingly, nanoparticles (Kumar et al., 2023) do not show strong accumulation in the heart of the *adult* mouse where EMT is no longer taking place. Our findings on nanoplastic biodistribution in reference to the heart is interesting in the light of recent research suggesting that MPs are a risk factor in cardiovascular disease (Zhu et al., 2023). Furthermore, MPs have been found in human heart tissue (Yang et al., 2023) and have been linked to atherosclerosis (Marfella et al., 2024). Finally, we have previously reported that nanoplastics cause cardiac defects in the chick embryo [9.].

We believe that NPs also cross the liver endothelium because we observed fluorescent NPs on the surface of the endothelium at stage 25, but between the endothelium and the hepatocytes at stage 28. In the neural tube (the primordium of the central nervous system), we observed fluorescent NPs in the neural epithelium itself. However, it is possible that these NPs were intravascular, because capillaries have already started vascularising the neural tube at stage 21 (Kurz et al., 1996).

Understanding biodistribution is the first step in understanding interactions of nanoplastics in living chicken embryos. In view of our finding that NPs show strong accumulation in the heart, liver and kidneys, it will be important to study these organs further when looking at NP biodistribution. The chicken embryo is a valuable animal model in developmental toxicity (Stark et al., 2019), and we suggest that future research could integrate developmental toxicity with a study of cellular-molecular mechanisms in this species.

The biodistribution (and other biological interactions) of nanoparticles are likely to be influenced by their size, surface charge, hydrophobicity, composition and their surface-bound biomolecules or 'corona' etc. (Eldridge et al., 1990; Jani et al., 1992; Gao et al., 2023; Röcker et al., 2009). When dealing with tagged particles, it is important to consider the impact of the taggant, as it can potentially change their physicochemical characteristics and behaviour *in vivo* (Robson et al., 2018). In this study, we used different sizes of NP (150 nm and 1 μm), different surface treatments (carboxylated or non-carboxylated) and different taggants (europium or fluorescent label). The differences in size and taggant had no detectable effect on the biodistribution of NPs in the tissues of the chicken embryo after injection into the vitelline vein. We also used different quantitative methods for studying the biodistribution of NPs (quantification of Eu-NPs by ICMPS and of NMF-NPs by fluorescent intensity analysis) and these different techniques were in agreement in showing particularly high levels of NPs in the kidneys, heart and liver.

5. Conclusion

We have described the biodistribution of fluorescent and europium-tagged PS-NPs injected intravenously in the chicken embryo. Significantly, our analyses used different methodologies but were consistent in showing a relatively high level of NPs in the kidneys, heart and liver. We also provide evidence that NPs can cross epithelia in at least the liver and heart. It has previously been reported that PS-NPs can cause cardiac defects in the chicken embryos (Wang et al., 2023). Our current findings show that such defects may not only arise from damage to the cardiac neural crest as previously reported (Wang et al., 2023), but possibly also from an effect on cushion tissues (based on their biodistribution). Our results advance our understanding of the interactions of nanoplastics with tissues *in vivo*. This knowledge advances our understanding of the biodistribution of NPs. Such information may be useful to the field of nanomedicine, both in understanding the potentially beneficial properties of nanoplastics, and the risks in terms of toxicity.

CRediT authorship contribution statement

Meiru Wang: Writing – review & editing, Writing – original draft, Visualization, Supervision, Methodology, Investigation, Data curation, Conceptualization. **Shuhao Chen:** Writing – review & editing, Writing – original draft, Visualization, Validation, Data curation. **Shixiong Cheng:** Writing – review & editing, Visualization, Methodology, Investigation, Data curation, Conceptualization. **Tom A.P. Nederstigt:** Writing – review & editing, Writing – original draft, Validation, Methodology, Formal analysis. **Robert E. Poelmann:** Writing – review & editing, Supervision, Formal analysis. **Marco C. DeRuiter:** Writing – review & editing, Visualization, Investigation. **Gerda E.M. Lamers:** Writing – review & editing, Visualization, Supervision, Methodology. **Joost J. Willemse:** Writing – review & editing, Software, Methodology. **Chiara Mascitelli:** Writing – review & editing, Visualization, Investigation. **Martina G. Vijver:** Writing – review & editing, Supervision, Resources, Funding acquisition. **Michael K. Richardson:** Writing – review & editing, Writing – original draft, Supervision, Project administration, Methodology, Investigation, Conceptualization.

Declaration of competing interest

The authors declare that they have no known competing financial interests or personal relationships that could have appeared to influence the work reported in this paper.

Data availability

Data will be made available on request.

Acknowledgements

Merijn de Bakker, Bert J. Wisse and Gio Ramanand are thanked for technical help. Ronald Limpens and Roman Koning from the Electron Microscopy Facility, Chemical Cell Biology Department, Leiden University Medical Center. We thank four anonymous reviewers for

improving our manuscript.

Funding sources

We are grateful to the European Research Council (grant number 101002123) for support to M.V. and T.A.P.N; and the Chinese Scholarship Council scholarship number 201908210335 for support to M.W.

Appendix A. Supplementary data

Supplementary data to this article can be found online at https://doi.org/10.1016/j.envint.2024.108723.

References

Abdolahpur Monikh, F., Hansen, S.F., Vijver, M.G., Kentin, E., Nielsen, M.B., Baun, A., et al., 2022. Can current regulations account for intentionally produced nanoplastics? Environ. Sci. Tech. 56 (7), 3836–3839.
Akdogan, Z., Guven, B., 2019. Microplastics in the environment: A critical review of current understanding and identification of future research needs. Environ. Pollut. 254, 113011.
Amato-Lourenço, L.F., Carvalho-Oliveira, R., Júnior, G.R., dos Santos, G.L., Ando, R.A., Mauad, T., 2021. Presence of airborne microplastics in human lung tissue. J. Hazard. Mater. 416.
Bakry, R., Vallant, R.M., Najam-ul-Haq, M., Rainer, M., Szabo, Z., Huck, C.W., Bonn, G. K., 2007. Medicinal applications of fullerenes. Int. J. Nanomed.
Ben-Shachar, G., Arcilla, R.A., Lucas, R.V., Manasek, F.J., 1985. Ventricular trabeculations in the chick embryo heart and their contribution to ventricular and muscular septal development. Circ. Res. 57 (5), 759–766.
Binnemans, K., Lenaerts, P., Driesen, K., Görller-Walrand, C., 2004. A luminescent tris (2-thenoyltrifluoroacetonato) europium (III) complex covalently linked to a 1, 10-phenanthroline-functionalised sol–gel glass. J. Mater. Chem. 14 (2), 191–195.
Boehnke, N., Straehla, J.P., Safford, H.C., Kocak, M., Rees, M.G., Ronan, M., et al., 2022. Massively parallel pooled screening reveals genomic determinants of nanoparticle delivery. Science 377 (6604), eabm5551.
Braet, F., Wisse, E., 2012. AFM imaging of fenestrated liver sinusoidal endothelial cells. Micron 43 (12), 1252–1258.
Brun, N.R., van Hage, P., Hunting, E.R., Haramis, A.G., Vink, S.C., Vijver, M.G., et al., 2019. Polystyrene nanoplastics disrupt glucose metabolism and cortisol levels with a possible link to behavioural changes in larval zebrafish. Commun Biol 2, 382.
Butler, K.S., Brinker, C.J., Leong, H.S., 2022. Bridging the in vitro to in vivo gap: using the chick embryo model to accelerate nanoparticle validation and qualification for in vivo studies. ACS Nano 16 (12), 19626–19650.
Chai, G., Hassan, A., Meng, T., Lou, L., Ma, J., Simmers, R., et al., 2020. Dry powder aerosol containing muco-inert particles for excipient enhanced growth pulmonary drug delivery. Nanomed. Nanotechnol. Biol. Med. 29.
Chen, Y., Feng, X., 2022. Gold nanoparticles for skin drug delivery. Int. J. Pharm.
Chen, T., Mori, Y., Inui-Yamamoto, C., Komai, Y., Tago, Y., Yoshida, S., et al., 2017. Polymer-brush-afforded SPIO nanoparticles show a unique biodistribution and MR imaging contrast in mouse organs. Magn. Reson. Med. Sci. 16 (4), 275–283.
Choudhury, M.I., Li, Y., Mistriotis, P., Vasconcelos, A.C.N., Dixon, E.E., Yang, J., et al., 2022. Kidney epithelial cells are active mechano-biological fluid pumps. Nat. Commun. 13 (1), 2317.
De Jong, W.H., Hagens, W.I., Krystek, P., Burger, M.C., Sips, A.J.A.M., Geertsma, R.E., 2008. Particle size-dependent organ distribution of gold nanoparticles after intravenous administration. Biomaterials 29 (12).
Delaney, S., Rodriguez, C., Sarrett, S.M., Dayts, E.J., Zeglis, B.M., Keinänen, O., 2023. Unraveling the in vivo fate of inhaled micro- and nanoplastics with PET imaging. Sci. Total Environ. 904, 166320.
Duman, R., Ertekin, T., Duman, R., Aslan, E., Sabaner, M.C., Cetinkaya, E., 2019. The novel model: Experimental optical coherence tomography-guided anterior segment imaging chick embryo model. Indian J. Ophthalmol. 67 (1), 54–58.
Eldridge, J.H., Hammond, C.J., Meulbroek, J.A., Staas, J.K., Gilley, R.M., Tice, T.R., 1990. Controlled vaccine release in the gut-associated lymphoid tissues. I. Orally administered biodegradable microspheres target the peyer's patches. J. Control. Release 11 (1–3).
Fatemifar, F., Feldman, M.D., Oglesby, M., Han, H.C., 2019. Comparison of biomechanical properties and microstructure of Trabeculae Carneae, papillary muscles, and myocardium in the human heart. J. Biomech. Eng. 141 (2).
Fattal, E., Tsapis, N., 2014. Nanomedicine technology: current achievements and new trends. Clin. Trans. Imaging 2 (1), 77–87.
Fernández, Y., Movellan, J., Foradada, L., Giménez, V., García-Aranda, N., Mancilla, S., et al., 2022. In vivo antitumor and antimetastatic efficacy of a polyacetal-based paclitaxel conjugate for prostate cancer therapy. Adv. Healthc. Mater. 11 (7), 2101544.
Ferreira, I., Venâncio, C., Lopes, I., Oliveira, M., 2019. Nanoplastics and marine organisms: What has been studied? Environ. Toxicol. Pharmacol. 67, 1–7.
Gamble, M., 2008. 9 - The Hematoxylins and Eosin. In: Bancroft, J.D., Gamble, M. (Eds.), Theory and Practice of Histological Techniques, sixth ed. Edinburgh, Churchill Livingstone, pp. 121–134.
Gao, J., Song, Q., Gu, X., Jiang, G., Huang, J., Tang, Y., et al., 2023. Intracerebral fate of organic and inorganic nanoparticles is dependent on microglial extracellular vesicle function. Nat. Nanotechnol. 1–11.
Gaylarde, C.C., Baptista Neto, J.A., da Fonseca, E.M., 2021. Nanoplastics in aquatic systems - are they more hazardous than microplastics? Environ. Pollut. 272, 115950.
Gewert, B., Plassmann, M.M., MacLeod, M., 2015. Pathways for degradation of plastic polymers floating in the marine environment. Environ. Sci. Processes Impacts 17 (9), 1513–1521.
Grinstein, M., Yelin, R., Herzlinger, D., Schultheiss, T.M., 2013. Generation of the podocyte and tubular components of an amniote kidney: timing of specification and a role for Wnt signaling. Development 140 (22), 4565–4573.
Habumugisha, T., Zhang, Z., Fang, C., Yan, C., Zhang, X., 2023. Uptake, bioaccumulation, biodistribution and depuration of polystyrene nanoplastics in zebrafish (Danio rerio). Sci. Total Environ. 893, 164840.
Hamburger, V., Hamilton, H.L., 1951. A series of normal stages in the development of the chick embryo. J. Morphol. 88 (1).
Hillier, L.W., Miller, W., Birney, E., Warren, W., Hardison, R.C., Ponting, C.P., et al., 2004. Sequence and comparative analysis of the chicken genome provide unique perspectives on vertebrate evolution. Nature 432 (7018), 695–716.
Hogers, B., DeRuiter, M.C., Baasten, A.M.J., Groot, A.C.G.-D., Poelmann, R.E., 1995. Intracardiac blood flow patterns related to the yolk sac circulation of the chick embryo. Circ. Res. 76 (5), 871–877.
Hu, Q., Wang, H., He, C., Jin, Y., Fu, Z., 2021. Polystyrene nanoparticles trigger the activation of p38 MAPK and apoptosis via inducing oxidative stress in zebrafish and macrophage cells. Environ. Pollut. 269, 116075.
Jani, P.U., McCarthy, D.E., Florence, A.T., 1992. Nanosphere and microsphere uptake via Peyer's patches: observation of the rate of uptake in the rat after a single oral dose. Int. J. Pharm. 86 (2–3).
Jia, Y., Jiang, Y., He, Y., Zhang, W., Zou, J., Magar, K.T., et al., 2023. Approved nanomedicine against diseases. *Pharmaceutics* 15, 3.
Johrden, L., Tenbusch, M., Lietz, R., Bonsmann, M.S.G., Niezold, T., Wildner, O., Bayer, W., 2013. Comparison of polystyrene nanoparticles and UV-inactivated antigen-displaying adenovirus for vaccine delivery in mice. Virol. J. 10.
Kamei, M., Carman, C.V., 2010. New observations on the trafficking and diapedesis of monocytes. Curr. Opin. Hematol. 17 (1), 43–52.
Kaur, H., Kumar, S., Kukkar, D., Kaur, I., Singh, K., Bharadwaj, L.M., 2010. Transportation of drug-(polystyrene bead) conjugate by actomyosin motor system. J. Biomed. Nanotechnol. 6 (3).
Keinänen, O., Dayts, E.J., Rodriguez, C., Sarrett, S.M., Brennan, J.M., Sarparanta, M., Zeglis, B.M., 2021. Harnessing PET to track micro- and nanoplastics in vivo. Sci. Rep. 11 (1), 11463.
Kessel, R.G., Kardon, R.H., 1979. Tissues and organs: a text-atlas of scanning electron microscopy. Freeman San Francisco, Calif., San Francisco, Calif.
Kopatz, V., Wen, K., Kovacs, T., Keimowitz, A.S., Pichler, V., Widder, J., et al., 2023. Micro- and nanoplastics breach the blood-brain barrier (BBB): biomolecular corona's role revealed. Nanomaterials (Basel) 13 (8).
Kopeček, J., Yang, J., 2020. Polymer nanomedicines. Adv. Drug Deliv. Rev. 156, 40–64.
Kumar, M., Kulkarni, P., Liu, S., Chemuturi, N., Shah, D.K., 2023. Nanoparticle biodistribution coefficients: A quantitative approach for understanding the tissue distribution of nanoparticles. Adv. Drug Deliv. Rev. 194, 114708.
Kurz, H., Gartner, T., Eggli, P.S., Christ, B., 1996. First blood vessels in the avian neural tube are formed by a combination of dorsal angioblast immigration and ventral sprouting of endothelial cells. Dev. Biol. 173 (1), 133–147.
Leslie, H.A., van Velzen, M.J.M., Brandsma, S.H., Vethaak, A.D., Garcia-Vallejo, J.J., Lamoree, M.H., 2022. Discovery and quantification of plastic particle pollution in human blood. Environ. Int. 163.
Li, P., Li, Q., Lai, Y., Yang, S., Yu, S., Liu, R., et al., 2023. Direct entry of micro(nano) plastics into human blood circulatory system by intravenous infusion. iScience 26 (12), 108454.
Li, J., Liu, X.G., Ge, R.L., Yin, Y.P., Liu, Y.D., Lu, W.P., et al., 2023. The ligation between ERMAP, galectin-9 and dectin-2 promotes Kupffer cell phagocytosis and antitumor immunity. Nat. Immunol. 24 (11), 1813–1824.
Liang, B., Zhong, Y., Huang, Y., Lin, X., Liu, J., Lin, L., et al., 2021. Underestimated health risks: polystyrene micro- and nanoplastics jointly induce intestinal barrier dysfunction by ROS-mediated epithelial cell apoptosis. Part. Fibre Toxicol. 18 (1), 20.
Liu, Z., Sokratian, A., Duda, A.M., Xu, E., Stanhope, C., Fu, A., et al., 2023. Anionic nanoplastic contaminants promote Parkinson's disease–associated α-synuclein aggregation. Sci. Adv. 9 (46), eadi8716.
Luo, Y., Li, L., Feng, Y., Li, R., Yang, J., Peijnenburg, W.J.G.M., Tu, C., 2022. Quantitative tracing of uptake and transport of submicrometre plastics in crop plants using lanthanide chelates as a dual-functional tracer. Nat. Nanotechnol. 17 (4), 424–431.
Manner, J., Merkel, N., 2007. Early morphogenesis of the sinuatrial region of the chick heart: a contribution to the understanding of the pathogenesis of direct pulmonary venous connections to the right atrium and atrial septal defects in hearts with right isomerism of the atrial appendages. Anat Rec (hoboken) 290 (2), 168–180.
Marfella, R., Prattichizzo, F., Sardu, C., Fulgenzi, G., Graciotti, L., Spadoni, T., et al., 2024. Microplastics and nanoplastics in atheromas and cardiovascular events. N. Engl. J. Med. 390 (10), 900–910.
Markwald, R.R., Fitzharris, T.P., Manasek, F.J., 1977. Structural development of endocardial cushions. AmJAnat 148 (1), 85–119.
Meides, N., Menzel, T., Poetzschner, B., Löder, M.G.J., Mansfeld, U., Strohriegl, P., et al., 2021. Reconstructing the environmental degradation of polystyrene by accelerated weathering. Environ. Sci. Tech. 55 (12), 7930–7938.
Mendoza, A., Osa, J.L., Basurko, O.C., Rubio, A., Santos, M., Gago, J., et al., 2020. Microplastics in the Bay of Biscay: An overview. Mar. Pollut. Bull.

Nie, J.-h., Shen, Y., Roshdy, M., Cheng, X., Wang, G., Yang, X., 2021. Polystyrene nanoplastics exposure caused defective neural tube morphogenesis through caveolae-mediated endocytosis and faulty apoptosis. Nanotoxicology 1–20.
Nikolic, S., Gazdic-Jankovic, M., Rosic, G., Miletic-Kovacevic, M., Jovicic, N., Nestorovic, N., et al., 2022. Orally administered fluorescent nanosized polystyrene particles affect cell viability, hormonal and inflammatory profile, and behavior in treated mice. Environ. Pollut. 305, 119206.
Paul, M.B., Fahrenson, C., Givelet, L., Herrmann, T., Loeschner, K., Böhmert, L., et al., 2022. Beyond microplastics - investigation on health impacts of submicron and nanoplastic particles after oral uptake in vitro. Microplastics Nanoplastics 2 (1), 16.
Primpke, S., Christiansen, S.H., Cowger, W., De Frond, H., Deshpande, A., Fischer, M., et al., 2020. Critical assessment of analytical methods for the harmonized and cost-efficient analysis of microplastics. Appl. Spectrosc. 74 (9), 1012–1047.
Qayyum, S.R., Webb, S., Anderson, R.H., Verbeek, F.J., Brown, N.A., Richardson, M.K., 2001. Septation and valvar formation in the outflow tract of the embryonic chick heart. Anat. Rec. 264 (3), 273–283.
Ragusa, A., Svelato, A., Santacroce, C., Catalano, P., Notarstefano, V., Carnevali, O., et al., 2021. Plasticenta: First evidence of microplastics in human placenta. Environ. Int.
Ragusa, A., Notarstefano, V., Svelato, A., Belloni, A., Gioacchini, G., Blondeel, C., et al., 2022. Raman microspectroscopy detection and characterisation of microplastics in human breastmilk. Polymers 14 (13).
Ranchod, T.M., Goldenberg, D.T., Trese, M.T., 2010. The physiological consequences of vitreous composition. Encyclopedia Eye.
Rashidi, H., Sottile, V., 2009. The chick embryo: hatching a model for contemporary biomedical research. Bioessays 31 (4), 459–465.
Rasmussen, S., Kjær Petersen, K., Kristiansen, M.K., Skallerup, J., Aboo, C., Thomsen, M. E., et al., 2022. Gold micro-particles for knee osteoarthritis. European J. Pain (United Kingdom) 26 (4).
Rice, W.L., Van Hoek, A.N., Păunescu, T.G., Huynh, C., Goetze, B., Singh, B., et al., 2013. High resolution helium ion scanning microscopy of the rat kidney. PLoS One 8 (3), e57051.
Robson, A.L., Dastoor, P.C., Flynn, J., Palmer, W., Martin, A., Smith, D.W., et al., 2018. Advantages and limitations of current imaging techniques for characterizing liposome morphology. Front. Pharmacol.
Röcker, C., Pötzl, M., Zhang, F., Parak, W.J., Nienhaus, G.U., 2009. A quantitative fluorescence study of protein monolayer formation on colloidal nanoparticles. Nat. Nanotechnol. 4 (9), 577–580.
Ross, W.D., Smith, J.A., 1910. The Works of Aristotle*: Historia animalium, by D.W. Thompson. 1910.* Clarendon Press.
Sangkham, S., Faikhaw, O., Munkong, N., Sakunkoo, P., Arunlertaree, C., Chavali, M., et al., 2022. A review on microplastics and nanoplastics in the environment: Their occurrence, exposure routes, toxic studies, and potential effects on human health. Mar. Pollut. Bull. 181, 113832.
Shan, S., Zhang, Y., Zhao, H., Zeng, T., Zhao, X., 2022. Polystyrene nanoplastics penetrate across the blood-brain barrier and induce activation of microglia in the brain of mice. Chemosphere 298, 134261.
Sharma, V.K., Ma, X., Lichtfouse, E., Robert, D., 2023. Nanoplastics are potentially more dangerous than microplastics. Environ. Chem. Lett. 21 (4), 1933–1936.
Stark, M.R., Ross, M.M., 2019. The chicken embryo as a model in developmental toxicology. In: Hansen, J.M., Winn, L.M. (Eds.), Developmental Toxicology: Methods and Protocols. Springer, New York, New York, NY, pp. 155–171.
Sun, W., Jin, C., Bai, Y., Ma, R., Deng, Y., Gao, Y., et al., 2022. Blood uptake and urine excretion of nano- and micro-plastics after a single exposure. Sci. Total Environ. 848, 157639.
Tang, Y., Zhao, R., Pu, Q., Jiang, S., Yu, F., Yang, Z., Han, T., 2023. Investigation of nephrotoxicity on mice exposed to polystyrene nanoplastics and the potential amelioration effects of DHA-enriched phosphatidylserine. Sci. Total Environ. 892, 164808.
Tian, X., Bunda, P., Ishibe, S., 2022. Podocyte endocytosis in regulating the glomerular filtration barrier. Front. Med.
Wachholz, G.E., Rengel, B.D., Vargesson, N., Fraga, L.R., 2021. From the farm to the lab: how chicken embryos contribute to the field of teratology. Front. Genet. 12.
Waheed, S., Li, Z., Zhang, F., Chiarini, A., Armato, U., Wu, J., 2022. Engineering nano-drug biointerface to overcome biological barriers toward precision drug delivery. J. Nanobiotechnol.
Wakai, S., Hirokawa, N., 1978. Development of the blood-brain barrier to horseradish peroxidase in the chick embryo. Cell Tissue Res. 195 (2), 195–203.
Wan, Y., Li, X., Slevin, E., Harrison, K., Li, T., Zhang, Y., et al., 2022. Endothelial dysfunction in pathological processes of chronic liver disease during aging. FASEB J. 36 (1), e22125.
Wang, X., Jia, Z., Zhou, X., Su, L., Wang, M., Wang, T., Zhang, H., 2023. Nanoplastic-induced vascular endothelial injury and coagulation dysfunction in mice. Sci. Total Environ. 865, 161271.
Wang, M., Rücklin, M., Poelmann, R.E., de Mooij, C.L., Fokkema, M., Lamers, G.E.M., et al., 2023. Nanoplastics causes extensive congenital malformations during embryonic development by passively targeting neural crest cells. Environ. Int. 173, 107865.
Wei, W., Li, Y., Lee, M., Andrikopoulos, N., Lin, S., Chen, C., et al., 2022. Anionic nanoplastic exposure induces endothelial leakiness. Nat. Commun. 13 (1), 4757.
Weinstein, J.E., Crocker, B.K., Gray, A.D., 2016. From macroplastic to microplastic: Degradation of high-density polyethylene, polypropylene, and polystyrene in a salt marsh habitat. Environ. Toxicol. Chem. 35 (7), 1632–1640.
Wenz, J.R., Peck, M.P., Murphy, M.J., 1992. Unilateral renal agenesis in chick embryos: a model for chronic renal insufficiency. Int. J. Dev. Biol. 36 (3), 445–450.
Yang, Y., Xie, E., Du, Z., Peng, Z., Han, Z., Li, L., et al., 2023. Detection of various microplastics in patients undergoing cardiac surgery. Environ. Sci. Technol.
Yee, M.S.L., Hii, L.W., Looi, C.K., Lim, W.M., Wong, S.F., Kok, Y.Y., et al., 2021. Impact of microplastics and nanoplastics on human health. Nanomaterials.
Zhang, Y., Wang, J., Huang, S., Zhu, X., Liu, J., Yang, N., et al., 2009. Systematic identification and characterization of chicken (Gallus gallus) ncRNAs. Nucleic Acids Res. 37 (19), 6562–6574.
Zhong, Y., Yang, Y., Zhang, L., Ma, D., Wen, K., Cai, J., et al., 2024. Revealing new insights: Two-center evidence of microplastics in human vitreous humor and their implications for ocular health. Sci. Total Environ. 921, 171109.
Zhu, L., Ma, M., Sun, X., Wu, Z., Yu, Y., Kang, Y., et al., 2023. Microplastics entry into the blood by infusion therapy: few but a direct pathway. Environ. Sci. Technol. Lett.
Zhu, X., Wang, C., Duan, X., Liang, B., Genbo, X.E., Huang, Z., 2023. Micro- and nanoplastics: A new cardiovascular risk factor? Environ. Int. 171, 107662.